This is the accepted manuscript made available via CHORUS. The article has been published as:

Local and long-range magnetic order of the spin-3/2 system CoSb_{2}O_{6}

A. B. Christian, A. Rebello, M. G. Smith, and J. J. Neumeier

Phys. Rev. B **92**, 174425 — Published 30 November 2015

DOI: 10.1103/PhysRevB.92.174425

Local and Long-Range Magnetic Order of the Spin-3/2 System $CoSb_2O_6$

A. B. Christian, A. Rebello, M. G. Smith, and J. J. Neumeier
Department of Physics, Montana State University, Bozeman, Montana 59717-3840, USA

The Co^{2+} ions of $CoSb_2O_6$ exhibit local magnetic order below ∼80 K followed by long-range antiferromagnetic order below T_N = 13.45 K. Analysis of the magnetic susceptibility above T_N using an Ising model of Co-Co dimers, yields a magnetic exchange coupling $J_\parallel/k_B = -10.603(6)$ K (k_B is the Boltzmann constant). The transition at T_N is accompanied by a spin gap in the heat capacity (Δ_2/k_B = 33.92(9) K). Highly anisotropic behavior of the thermal expansion is observed, and the influence of local magnetic order is evident. A critical exponent of $\alpha = 0.103(3)$ is obtained from analysis of the critical behavior of the heat capacity and thermal expansion near T_N, similar to the value expected for the three dimensional Ising universality class.

PACS numbers: 75.40.-s, 75.47.Lx, 65.40.De

I. INTRODUCTION

Fermions constrained to one dimension (1D) are known to exhibit boson-like behavior of some collective excitations.[1,2] This topic, referred to as Luttinger-liquid theory, is relevant beyond the purely-1D case[3] and it is applicable to mobile fermions and those constrained to lattice sites.[4] Luttinger-liquid behavior can be investigated in bulk solids, but purely-1D states never exist there because interchain interactions result in higher-dimensional behavior. For example, a 1D chain of magnetic moments would not exhibit long-range-magnetic order due to quantum fluctuations, but interchain coupling among a collection of chains can induce order.[3] The coupling of 1D chains leads to substantial mathematical complexity,[3,5] and a theoretical understanding is still developing. For example, the presence of simple perturbations, such as magnetic field, destroy the integrability.[6] Thus, the study of bulk compounds with 1D chains of magnetic moments is important for developing a better understanding of 1D physics.

Transition-metal oxides with the chemical formula AB_2O_6, where A is a 3d transition metal and B is either Sb or Ta, are an interesting class of compounds with 1D magnetic chains. In most cases, they possess a trirutile structure with the A^{2+} cations located at the corners and the B^{5+} cations forming two parallel sheets.[7] Their low-dimensional magnetic behavior is evident from experiments[8–12] and electronic structure calculations.[13,14] In the case of $CuSb_2O_6$, orbital order is believed to promote antiparallel ordering of the magnetic moments along the [110] direction at $z = 0$ and the $[1\bar{1}0]$ direction at $z = 1/2$, which is commonly referred to as the two-sublattice antiferromagnetic structure. Spin-exchange constants of $NiTa_2O_6$, obtained[14] from density functional theory (DFT), exhibit a dominant antiferromagnetic exchange along the same structural diagonals as $CuSb_2O_6$. In contrast, $MnSb_2O_6$ (trigonal crystal structure) possesses a cycloidal magnetic structure, where all spin-exchange constants are of similar magnitude.[15]

The fact that some of these compounds can possess one dimensional (1D) chains that are weakly coupled to one another was proven through observations of an anisotropic magnetocaloric effect (MCE)[12] in $NiTa_2O_6$ and $CoSb_2O_6$. The MCE is manifested as a downward shift of the peak in heat capacity C_P with application of magnetic field H. If H is applied parallel to the 1D chains of one sublattice, it is then perpendicular to the 1D chains of the second sublattice. This magnetic field orientation causes the peak in C_P at T_N to split into two distinct peaks. The complexity of the magnetism in $CuSb_2O_6$, $CoSb_2O_6$, and $NiTa_2O_6$ is further demonstrated in the C_P data above T_N by the presence of local magnetic order between ∼100 K and T_N = 8.7 K, 13.45 and 10.5 K, respectively.[11–14] In the case of $CuSb_2O_6$, C_P exhibits an energy gap below T_N, with magnitude Δ/k_B = 17.5 K (k_B is the Boltzmann constant), which is associated with the magnetic order, and leads to the elimination of a linear term in C_P existing above T_N.[11] Such analysis for $CoSb_2O_6$ will be reported below, and has yet to be investigated for $NiTa_2O_6$. The magnetic susceptibility χ of these compounds also exhibits behavior expected for one-dimensional spin-chain systems,[8,11,14,16] with broad peaks in χ above T_N.

Unambiguous identification of the magnetic structure associated with the antiferromagnetism of AB_2O_6 compounds has been challenging.[7,15–17] In the case of $CuSb_2O_6$, Nakua and Greedan[17] proposed two magnetic structures based on powder neutron diffraction data. One of these structures is the two-sublattice (or orthogonal) AFM structure, which describes the copper magnetic moments ordered antiparallel along [110] at $z = 0$ and $[1\bar{1}0]$ at $z = 1/2$. Gibson et al.[18] reported neutron diffraction measurements on single crystals and concluded that the moments ordered in a similar manner, but with a slight tilting to account for anisotropy in the magnetic susceptibility between the a- and b-axes below the Néel temperature. Kato *et al.*[16] utilized neutron diffraction on single crystals and determined that the magnetic moments aligned ferromagnetically along [010] with moments of adjacent chains aligned antiparallel, thus forming a magnetic wave vector (π/a, 0, π/c). More recent experiments[19] agree with Kato *et al.* The latter two investigations appear to be the most detailed, and they are corroborated by magnetic susceptibility[12] and torque

magnetometry[20] data below T_N. It thus appears that the structure obtained by Kato *et al.* agrees best with the available data. This structural model, however, disagrees with the magnetic structure suggested from calculated spin-exchange constants.[13] In the case of $NiTa_2O_6$, Law et al.[14] determined that the dominant AFM exchange path is along [110] at $z = 0$ and [1$\bar{1}$0] at $z = 1/2$ which describes the same AFM two-sublattice structure as above. Ehrenberg et al.,[21] on the other hand, reported a different magnetic structure in which the magnetic moments collinearly aligned parallel to [110] (without a sublattice rotated by 90°). However, the anisotropic MCE[12] described above is consistent only with the two-sublattice AFM structure.

The subject of the present study is $CoSb_2O_6$. It crystallizes[22] in a tetragonal, trirutile structure with space group $P4_2/mnm$ and lattice parameters $a = 4.6495$ Å and $c = 9.2763$ Å. It is an electrical insulator with electrical conductivity[23] $\leq 10^{-7}$ $(\Omega{\cdot}\mathrm{cm})^{-1}$ at 295 K. Long-range AFM order occurs below Néel temperature $T_N = 13.45$ K; this order appears consistent with the two-dimensional Ising model.[22] The magnetic structure of $CoSb_2O_6$ was reported as similar to that of $FeTa_2O_6$.[22] However, two different magnetic structures have been proposed for $FeTa_2O_6$,[9] one of which is identical to the two-sublattice structure introduced above. Our previous report[12] explored the anisotropy of the magnetic susceptibility of single-crystal $CoSb_2O_6$, concluding that the two-sublattice AFM structure seems appropriate for $CoSb_2O_6$. Furthermore, the presence of one-dimensional magnetic chains was convincingly revealed through the anisotropic MCE.

In this report, an exploration of the physical properties of single-crystalline $CoSb_2O_6$ is presented. The magnetic susceptibility χ reveals significant anisotropy along with a broad peak in its temperature dependence that is characteristic of 1D AFM spin-chain systems. Curie-Weiss analysis indicates that the Co^{2+} ion is in the high-spin state, $S = 3/2$. The $\chi(T)$ data are also analyzed with a model for 1D spin-chain systems consisting of $S = 3/2$ dimers. The results yield a value for the coupling along the 1D chain of $J_\parallel/k_\mathrm{B} = -10.603(6)$ K. Heat capacity data reveal a significant loss of magnetic entropy upon cooling below 80 K, which is well above $T_N = 13.45$ K; this indicates the presence of a substantial amount of local magnetic order above T_N. This local order coalesces into long-range antiferromagnetism at T_N for which a critical exponent consistent with the three dimensional (3D) Ising model is observed. Thus, the transition at T_N can be viewed as a crossover from local, probably 1D, to 3D antiferromagnetism. High-resolution thermal expansion measurements are also presented. They exhibit significant anisotropy, including a negative thermal expansion coefficient along the c-axis below 80 K. Comparison to thermal expansion measurements of non-magnetic $ZnSb_2O_6$ allows association of the unusual thermal expansion of $CoSb_2O_6$ with its local magnetic order.

II. SAMPLE PREPARATION AND MEASUREMENT DETAILS

Polycrystalline samples were prepared using Co_3O_4 and Sb_2O_3. A slight excess (about 5 percent) of Sb_2O_3 was added to prevent[22] formation of $Co_7Sb_2O_{15}$. The starting materials were mixed, pelletized, and placed in an alumina crucible; the sample was warmed from 400°C at 50°C/day to 1050°C, and held there for 3 days. One regrinding and re-firing was performed to obtain a pure phase, which was confirmed using x-ray diffraction. The crystal structure is tetragonal with lattice parameters that agree with prior work.[22]

For the single-crystal growth, one gram of $CoSb_2O_6$ powder was placed in a 1 cm diameter, 15 cm long quartz tube (1 mm wall thickness) along with 100 mg of $TeCl_4$, the source of Cl vapor.[24] The tube was evacuated to a pressure of 1.3×10^{-3} mbar before being sealed. It was held at a temperature of 220 °C for one hour, then brought to 380 °C at a rate of 50 °C/h. After remaining at this temperature for an hour, the temperature was increased to 930 °C at 183 °C/h where it was held for 200 h, after which it was cooled to room temperature in 15 h. The thermal gradient across the tube length was ∼4.5 °C/cm. The Cl vapor transports the $CoSb_2O_6$ from the hot side of the tube to the cool side, where single-crystals form. The crystals have the expected crystal structure,[22] are typically 3 to 5 mg in mass, dark brown in color, and often formed as bicrystals. Bicrystal boundaries were identified during the orienting process, in which Laue x-ray diffraction was employed. The unwanted secondary crystal was removed via polishing.

Magnetic susceptibility and heat capacity were measured using a Quantum Design Physical Properties Measurement System (PPMS). The susceptibility was measured for three crystals ($m_1 = 3.71$ mg, $m_2 = 4.74$ mg, and $m_3 = 5.67$ mg) using a constant 2 kOe magnetic field over a temperature range of 2 to 300 K; field is applied in the same direction as the moment measurement. The data obtained from the three crystals agreed well. Heat capacity was measured on a polycrystalline sample of $CoSb_2O_6$ of mass 22.77 mg and on all three single crystals. $ZnSb_2O_6$ was utilized as a non-magnetic analog for analysis purposes. Its preparation was reported previously.[11]

Thermal expansion measurements were performed on samples 1 and 2 (with dimensions $a \times b \times c$ equal to 1.18 × 0.55 × 0.92 mm^3 and 1.20 × 0.85 × 0.81 mm^3) using a dilatometer cell constructed of fused quartz,[25] which can determine changes in length at a resolution of up to 0.1 Å. Each curve presented herein is composed of about 1800 data points, with a spacing of 0.2 K. The data for the linear thermal expansion were fitted using a method described previously[26] prior to calculating the thermal expansion coefficient. Thermal expansion data for the two crystals agree well.

III. RESULTS AND ANALYSIS

A. Magnetic Measurements and Analysis

Magnetic susceptibility χ at $H = 2000$ Oe is shown in Fig. 1. The data were corrected for the temperature-independent diamagnetism associated with the core electrons ($\chi_{dia} = -112 \times 10^{-6}$ emu/mol).[27] They reveal a broad peak, which is typical for systems possessing 1D chains of antiferromagnetically-coupled spins. Below this peak, a transition due to long-range antiferromagnetic order is observed at $T_N = 13.45$ K; this region is enlarged in the inset of Fig. 1. An obvious anisotropy exists between the *a*- and *c*-axes. Cooling in magnetic field (FC) and cooling in zero magnetic field, followed by application of field (ZFC), exhibited no difference in $\chi(T)$. This conflicts with a prior report,[28] where the FC susceptibility differed from the ZFC susceptibility below the broad peak. The authors attributed this behavior to spin-freezing, which must be associated with the polycrystalline nature of the samples.

Analysis of $\chi(T)$ was conducted using the Curie-Weiss equation $\chi = C/(T-\theta)+\chi_0$, where C is the Curie-Weiss constant, θ is the Curie-Weiss temperature, and χ_0 is a temperature-independent constant. The Curie-Weiss constant is given by

$$C = \frac{Ng^2\mu_B^2 J(J+1)}{3k_B} = \frac{N\mu_{\rm eff}^2}{3k_B}, \qquad (1)$$

where N is the number of moles, g is the Landé g-factor, μ_B is the Bohr magneton, and J is the total angular momentum. The data were fitted for $T > 130$ K, which is above the region ($T < 80$ K) where local 1D antiferromagnetic order appears (see discussion of heat capacity data below). The fits are shown by the dashed lines in Fig. 2. The values $\mu_{\rm eff} = 4.617(1)\mu_B$ and $\chi_0 = 3.36(3)\times10^{-4}$ emu/mole Oe for the *a*-axis, and $\mu_{\rm eff} = 4.606(3)\mu_B$ and $\chi_0 = 3.31(6)\times10^{-4}$ emu/mole Oe for the *c*-axis, were obtained from the fits. The orbital-angular momentum is typically quenched for 3d ions,[29] making $J = S$ in Eq. (1). The observed magnetic moment reveals that the Co^{2+} ions are in the $S = 3/2$ state with $g_a = 2.384(1)$ and $g_c = 2.379(1)$ for the a and c axes, respectively. Since the values of $\mu_{\rm eff}$ are identical, within error, the single-ion anisotropy is negligible; this is consistent with the minimal variation (about 2%) of Co-O bond-lengths within the CoO_6 octahedra,[12] which leads to a nearly-cubic crystal electric field. Deviation from $g = 2.00$ is common for 3d elements with their d-shells more than half full, and is associated with the spin-orbit interaction. A typically observed value[30] for $\mu_{\rm eff}$ of Co^{2+} with $S = 3/2$ is $4.8\mu_B$, close to what is observed here. For comparison, $\mu_{\rm eff} = 4.62(1)\mu_B$ was reported for a polycrystal.[22] Curie-Weiss temperatures $\theta_a = \theta_b = -22.2$ K and $\theta_c = -44.1$ K were obtained in the fitting. The average of these is similar to $\theta = -32.4$ K reported for a polycrystalline sample.[22] The negative values of θ indicate antiferromagnetic correlations.

The temperature-independent constant $\chi_0 \approx 3.3 \times10^{-4}$ emu/mole Oe is attributed to Van-Vleck paramagnetic susceptibility. Its magnitude is comparable to the literature value[31] $\chi_{VV} \sim 4.0\times10^{-4}$ emu/mole Oe. A Van-Vleck susceptibility of $\chi_{VV} \sim 9\times10^{-3}$ emu/mole Oe was obtained for the Co^{2+} ion from magnetization data for H > 30 tesla measured on a sample of $Ba_3CoSb_2O_9$,[32] but the magnitude seems far too large when compared to this and earlier work.[31]

For an antiferromagnet, χ is expected to approach zero as $T \to 0$ for H applied along the easy axis of magnetization.[33] Fig. 1 shows data for H along a and c. Clearly the easy axis does not lie along c. Within the a-b plane, χ was measured for $H \parallel b$ (i.e. H applied parallel to the [010] crystallographic direction), $H \parallel [110]$, and $H \parallel [1\bar{1}0]$. All of these measurements revealed data identical to the $H \parallel a$ data shown in Fig. 1. This behavior of χ as $T \to 0$ implies that the moments are *not* aligned parallel to any of the axes measured within the a-b plane. This is further evidence for the two-sublattice structure described in the introduction.

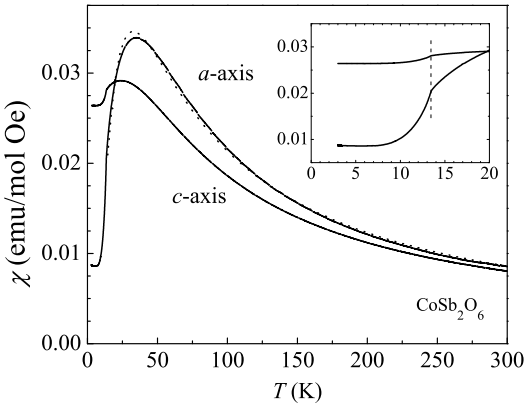

FIG. 1: Magnetic susceptibility versus temperature for $CoSb_2O_6$ at 2000 Oe. The dashed line is a fit using Eq. (2) plotted for T >14 K. The inset shows an expanded view of the data near $T_N = 13.45$ K (vertical dashed line).

A broad peak in χ is characteristic of 1D spin-chain systems, and is generally modeled with the Bonner-Fisher theory[34] for $S = 1/2$ using the anisotropic Ising-Heisenberg Hamiltonian. Unfortunately, no analogous model exists for spin-chains with $S = 3/2$, due to the computational complexities associated with the additional degrees of magnetic freedom. We have therefore calculated an expression for $\chi_\parallel$ (the susceptibility of the magnetic moments measured parallel to the applied field, called here $H_\parallel$) for a $S = 3/2$ Ising model by following the method of Carlin[35,36] for $S = 1/2$ dimers. In this model, the spins have only two orientations, up or down. The eigenvalues of $S_\parallel$ for a single Co^{2+} ion are $+\frac{3}{2}$, $+\frac{1}{2}$, $-\frac{1}{2}$, and $-\frac{3}{2}$. A dimer, therefore, has a total of 16 possible states. The partition function Z for this system can

easily be written down, and differentiated according to $M = Nk_BT(\partial lnZ/\partial H_\parallel)_T$, to obtain the magnetization M. Differentiation with respect to the magnetic field and taking the low-field limit leads to the final result

$$\chi_\parallel = \frac{Ng^2\mu_B^2}{2k_BT}\frac{e^{\frac{3J_\parallel}{k_BT}}(2+e^{\frac{2J_\parallel}{k_BT}}+8e^{\frac{3J_\parallel}{k_BT}}+9e^{\frac{6J_\parallel}{k_BT}})}{1+2e^{\frac{3J_\parallel}{k_BT}}+e^{\frac{4J_\parallel}{k_BT}}+e^{\frac{5J_\parallel}{k_BT}}+2e^{\frac{6J_\parallel}{k_BT}}+e^{\frac{9J_\parallel}{k_BT}}}. \quad (2)$$

The parameter $J_\parallel$ represents the coupling energy between the two magnetic moments and the factor of 2 in the denominator is required to refer to a mole of magnetic ions.

The fit using Equation 2 is shown in Fig. 1 as a dashed line. The fit's quality is good, with the exception of the slight offset of the peak. The values $g_\parallel = 2.4442(5)$ and $J_\parallel/k_B = -10.603(6)$ K were obtained. The negative sign indicates antiferromagnetic coupling. The value of g is comparable to the value obtained from Eq. (1). The magnitude of $J_\parallel$ is comparable to values reported for polycrystalline $CoSb_2O_6$ and $CoTa_2O_6$, which were stated to be consistent with the anisotropic square planar Ising model.[22] It is apparent in Fig. 1 that the peak in χ for the c-axis data occurs at 23.6 K while the peak for the a-axis data occurs at 34.3 K. This reflects a preference for the locally-ordered magnetic moments (dimers) to lie in the a-b plane. When $H \parallel c$, more thermal energy must be removed before the susceptibility drops upon cooling, which would signal the presence of more dimers with spins pointing along H.

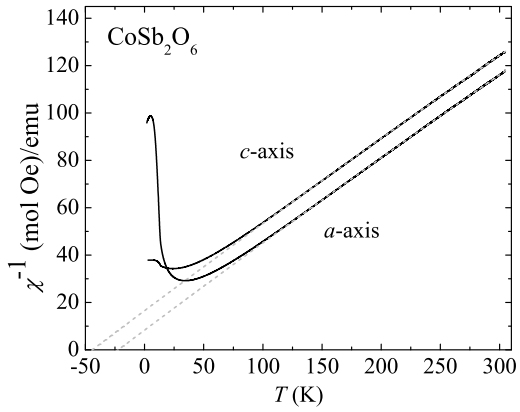

FIG. 2: Plot of χ^{-1} versus temperature at 2000 Oe. The dashed lines are linear fits upon which the Curie-Weiss analysis is based. These line were extrapolated to illustrate the T intercepts.

Magnetization of the crystal with m= 4.74 mg (sample 2) was measured from 0 to 9 tesla at 3 K (see Fig. 3) in order to search for a spin-flop transition, which is observed in $CuSb_2O_6$.[11] The data reveal a linear trend for $H \parallel c$. A minor deviation from linearity beginning above 7 tesla for $H \parallel a$ is observed. The a-axis data in Fig. 3 contain three separate measurements, for field applied along the [100], [010], and [110] crystallographic directions. The data lie directly on top of one another. The slight deviation at higher fields for the $H \parallel a$ data may be caused by the known shift in T_N to lower temperature when an applied field has a component parallel to the spin-chains within one of the sublattices.[12] No deviation would be expected for $H \parallel c$ since no shift in T_N with H occurs.

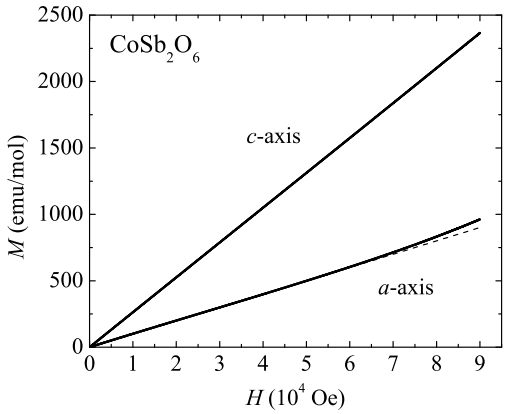

FIG. 3: Magnetic moment versus magnetic field at $T = 3$ K. The c-axis data are linear while the a-axis data deviate slightly from linearity (shown by the dashed line) at high field.

B. Heat Capacity and Thermal Expansion Measurements and Analysis

The heat capacity of $CoSb_2O_6$ is shown in Fig. 4(a). The phase transition at $T_N = 13.45$ K is clearly visible. Fitting with the equation $C_P/T = \gamma + \beta T^2$ for the polycrystalline sample over the range 24 K $< T <$ 37 K yields $\gamma = 204(1)$ mJ/mol K^2 and $\beta = 0.096(1)$ mJ/mol K^4 with a Debye temperature of $\Theta_D \equiv [(12\pi^4 N_i R)/(5\beta)]^{1/3} = 567(2)$ K, where N_i is the number of ions per formula unit and R is the gas constant. The same analysis for sample 3 yields $\gamma = 203(4)$ mJ/mol K^2, $\beta = 0.076(3)$ mJ/mol K^4 and $\Theta_D = 613(8)$ K. Note that $CoSb_2O_6$ is an electrical insulator,[23] so the γ term is *not* associated with the presence of conduction electrons. The heat capacity of $ZnSb_2O_6$ is also shown in Fig. 4(a); fitting results for these data can be found in Ref. 11. The C_P data of $ZnSb_2O_6$, which is non-magnetic, were subtracted from the $CoSb_2O_6$ data in order to isolate the magnetic contributions to the heat capacity; the result, δC_P, is plotted in Fig. 4.

An asymmetric peak with a long tail is observed in $\delta C_P/T$ (Fig. 4(b)), which goes to zero near 80 K, signaling the temperature below which local magnetic order begins to occur. The area under this curve is the magnetic entropy ΔS_m, which is shown in the inset of Fig. 4(b). The saturation value for the magnetic entropy should be $R\ln(2S+1) = 11.526$ J/mol K, where $S = 3/2$ and R is the ideal gas constant. The observed ΔS_m saturates at 7.64 J/mol K, which is 66.3% of the theoretical value for

spin 3/2. The loss of entropy upon cooling from 80 K to T_N is significant, 5.68 J/mol K (or 49.3% of the theoretical value for $S = 3/2$), which indicates that nearly half of the magnetic moments are engaged in local magnetic order *prior* to the onset of long-range magnetic order below T_N. This is consistent with the modeling of the magnetic susceptibility through Equation 2. A significant amount of local magnetic order above T_N was also observed[11] in $CuSb_2O_6$.

The presence of thermal excitations above T_N are evidenced by the linear term in C_P. Since this term is not due to conduction electrons, it seems reasonable to assume that its origin lies with magnetic excitations associated with the local magnetic order observed above T_N. In comparing the C_P data of $CoSb_2O_6$ and $CuSb_2O_6$, two main differences arise. First, the observed value of γ is significantly larger in $CoSb_2O_6$ (203(4) mJ/mol K versus 58.7(7) mJ/mol K). Second, although the linear term vanishes rapidly below T_N (see Fig. 4(a) and Ref. 11), in $CuSb_2O_6$ δC_P follows the simple form $\delta C_P \sim exp(-\Delta/k_BT)$ below T_N (with $\Delta/k_B = 17.48(6)$ K).[11] In the case of $CoSb_2O_6$, the plot of $\ln(\delta C_P)$ versus $1/T$ (inset of Fig. 4(a)) is not linear over the entire range below T_N, and requires a more complicated analysis. The data in this region were fitted with the equation

$$\delta C_P = A_1 T exp(-\Delta_1/k_BT) + A_2 T^3 exp(-\Delta_2/k_BT). \quad (3)$$

The first term is associated with the decay of the linear-in-T excitations observed above T_N. These are probably due to the regions of the sample that remain unordered below T_N. The second term is the dominant one; it represents antiferromagnetic magnons that possess a gap in their excitation spectrum.[37] The constant prefactors A_1 = 13.3(7) mJ/mol K^2 and A_2 = 0.0544(4) mJ/mol K^4. The energy gaps obtained from the fitting are Δ_1/k_B = 1.49(26) K and Δ_2/k_B = 33.92(9) K. The fit is shown in the inset of Fig. 4(a) by the solid line.

Thermal expansion measurements were performed along each of the three axes of sample 1 and sample 2 over a temperature range from 5 to 300 K. The change in sample length ΔL was normalized to the length at 300 K, L_{300}. It is plotted versus T in Fig. 5(a). Measurements along the a and b axes agree well, as expected for a sample with a tetragonal crystal structure. Comparison of the expansions along a and c reveals significant anisotropy, with the expansion along a about 1.75 times larger than the expansion along c over the measured temperature range. A change in slope of $\Delta L/L_{300}$ is apparent at 13.45 K for both axes (see upper insets in Fig. 5(a)). This is associated with the antiferromagnetic phase transition. Since a change in slope is observed, rather than a jump, the phase transition appears to be continuous (second-order) in nature. The feature at T_N along the a-axis is about 33 times larger than the feature along c, indicating that the coupling between the lattice and the magnetic order is stronger within the a-b plane than along c.

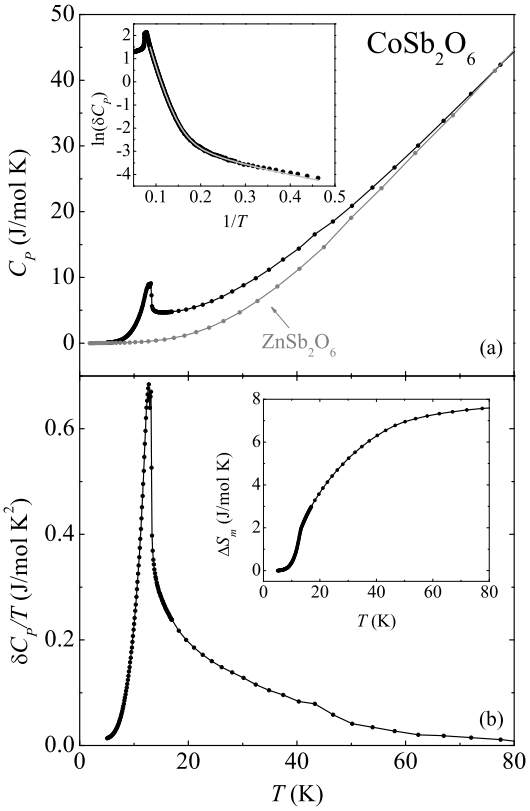

FIG. 4: (a) Heat capacity (C_P) for $CoSb_2O_6$ and the non-magnetic analog $ZnSb_2O_6$. The upper inset shows a natural log versus $1/T$ plot of the difference between the heat capacities of $CoSb_2O_6$ and $ZnSb_2O_6$ (δC_P); the solid line is a fit using Equation 3. (b) $\delta C_P/T$ is plotted versus T. The area under this curve is the magnetic entropy. It is shown in the inset.

The thermal expansion coefficients μ were obtained by taking the temperature derivative of the $\Delta L/L_{300}$ data; they are shown in Fig. 5(b). Also plotted are μ along a and c for the non-magnetic analog compound $ZnSb_2O_6$; note that $CoSb_2O_6$ and $ZnSb_2O_6$ both have tetragonal crystal structures and their lattice parameters differ by 1.7 % or less. The thermal expansion coefficients of these two compounds have similar values near 300 K, but deviate markedly as the temperature is lowered below ∼180 K. This difference must be associated with the presence of the magnetic ions, and the existence of local magnetic order as revealed in the ΔS_m data in Fig. 4(b).

Thermal expansion in solids results from anharmonic contributions to the elastic potential, with the pair potentials between neighboring atoms playing an important role in this many-body potential.[38] In $CoSb_2O_6$, local 1D magnetic order occurs on cooling below ∼80 K. This local magnetic order would directly affect the pair potentials in ordered regions of the sample,[38] which in turn could dramatically alter the phonon spectrum, especially given the large fraction of Co ions participating in magnetic order. We believe that the local magnetic order along the Co-O-O-Co chains leads to anharmonicity in some

lattice vibrations, and the very different behavior of μ for $CoSb_2O_6$ below 180 K when compared to $ZnSb_2O_6$. Below ∼40 K the thermal expansion coefficients change behavior because such a large proportion of the spins are ordered that the anharmonic contributions reduce upon further cooling, which leads to a decrease in the magnitude of μ. The negative thermal expansion along c is in strong contrast to the behavior along a, and is probably connected to the 1D behavior between T_N and 80 K, and anharmonic lattice vibrations that specifically affect μ along this direction. $CuGeO_3$ also exhibits[39] a prominent correlation between thermal expansion and the formation of 1D magnetic correlations.

The antiferromagnetic phase transition appears as a peak in the thermal expansion coefficient, as expected for a continuous phase transition. This temperature region is highlighted in the inset of Fig. 5(b). The peak associated with the phase transition for the c-axis is extremely small. For the a-axis data, a small double-peak is evident in μ, which is associated with a change in the sample warming rate.[40] The heat capacity in the immediate vicinity of a continuous phase transition can be written as[41]

$$C_P = T\left(\frac{\partial S}{\partial T}\right)_{T_N} + \nu T\Omega\left(\frac{\partial P}{\partial T}\right)_{T_N}, \qquad (4)$$

where S, P, ν, and Ω are the molar entropy, pressure, molar volume, and volume thermal expansion coefficient, respectively. The subscript T_N denotes that the equation is valid near the Néel temperature. The molar volume is $\nu = 6.864\times10^{-5}$ m^3/mol and Ω is taken to be the sum of the linear expansion coefficients $(2\mu_a+\mu_c)$ near T_N. The first term in Eq. (4) is linear. It can be subtracted from C_P to yield $C_P^* \equiv C_P - a - bT$. With $\nu/\lambda = dT_N/dP$, C_P^* scales with $\lambda\Omega T$. The values a, b, and λ are chosen such that the $\lambda\Omega T$ and C_P^* data have the best possible overlap. This is achieved (see Fig. 6) with a = 0.2 J/mol K, b = -0.06 J/mol K^2, and $\lambda = 1.7\times10^5$ J/mol K, which yields dT_N/dP = 0.40 K/GPa. We are unaware of any direct measurements of dT_N/dP at this time, with which to compare this value. The good overlap of the C_P^* and $\lambda\Omega$T in the vicinity of T_N (see Fig. 6) suggests that the phase transition at T_N is continuous.

The sharpness of the peak in C_P in sample 2 was observed to be very broad, as illustrated in Fig. 6, where a double-peak is evident; a double-peak was also observed in the polycrystalline sample as well (not shown). Measurement of C_P in magnetic field on single crystals revealed[12] that field can split the peak in C_P into two peaks, depending upon the orientation of the magnetic field with respect to the crystallographic axes. In this case, since a magnetic field was not present, the appearance of two peaks is probably associated with disorder.

The C_P^* data of sample 3 have been analyzed in the vicinity of the phase transition T_N to determine the heat capacity critical exponent α. The singularity in heat capacity around a phase transition originates from a non-

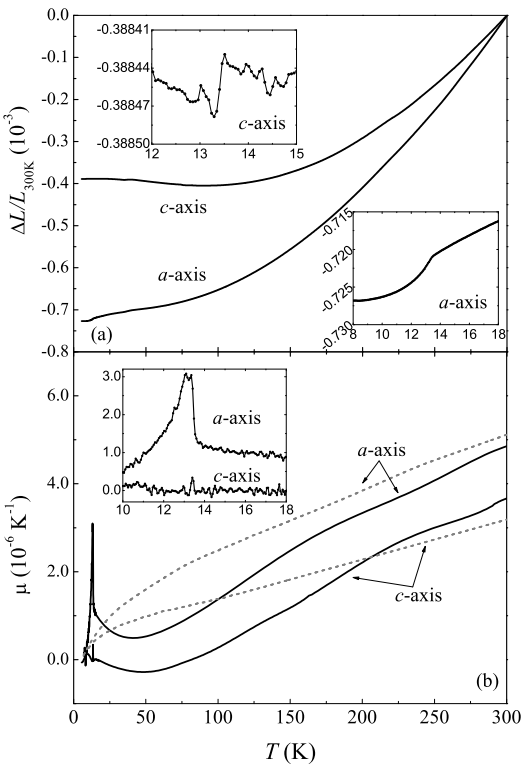

FIG. 5: (a) Linear thermal expansion normalized to the length at 300 K. The insets reveal the region near T_N = 13.45 K. (b) Thermal expansion coefficients found by taking the temperature derivatives of the data in the top panel. The dashed lines reveal the thermal expansion coefficients of the non-magnetic compound $ZnSb_2O_6$. The inset is the region near T_N.

analytic term in the thermodynamic free energy and can be asymptotically described[41] by a function of the form

$$C_P^* = \left(\frac{A_\pm}{\alpha_\pm}\right)|t|^{-\alpha_\pm} + B_\pm + Dt, \qquad (5)$$

where t is the reduced temperature $t \equiv |T - T_N|/T_N$; $A_\pm$, $B_\pm$, and D are constants; and $\alpha_\pm$ is the critical exponent.[41,42] The subscripts denote values of the parameters above (+) and below (−) T_N. The value for α can be determined from the C_P data by plotting $\log(C_P^* - B_\pm - Dt)$ against $\log(t)$ and adjusting fit parameter values until the regions above and below the phase transition become linear, with similar slopes. For a continuous phase transition, $\alpha_+ \approx \alpha_-$. This was achieved over two decades[43] in t (see the inset of Fig. 6) with $B_+ = -4.5$ J/mol K, $B_- = -45$ J/mol K, D = 5 J/mol K, and T_N = 13.5 K, resulting in A_+ = 0.2290(20) J/mol K, A_- = 0.4986(76) J/mol K, α_+ = 0.1062(9), and α_- = 0.100(2) (averaging to α = 0.103(3)). Data for samples 1 and 3 were used in the analysis. The obtained α value is close to α = 0.110(1), which is associated with the three-dimensional ferromagnetic Ising universality class.[44] Note that calculations of critical ex-

ponents for a given universality class usually assume a ferromagnetic model but there is reason to believe that they are also valid for antiferromagnets.[45,46] Some amplitude ratios are predicted to be universal quantities that should be identical for all systems in a given universality class.[47] For the 3-D Ising model, A_+/A_- is predicted to be 0.523(9),[48] the obtained value of $A_+/A_- = 0.459(8)$ is close to that prediction. Similarities to an Ising model are not surprising since Co^{2+} ions provide some of the best examples of Ising systems.[35]

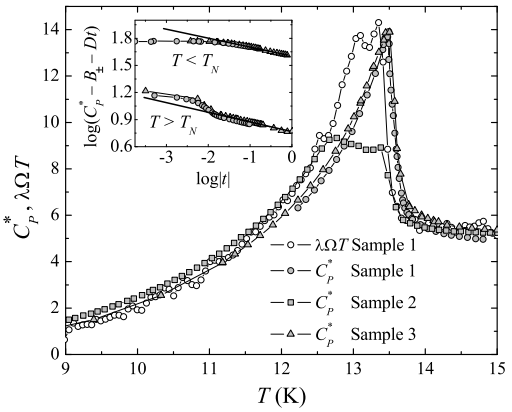

FIG. 6: Plot of C_P^* and $\lambda\Omega T$ versus temperature illustrating the overlap of heat capacity and volume thermal expansion coefficient data in the vicinity of T_N. The double-peak nature of C_P and Ω is also evident in this figure. The inset shows the critical behavior of C_P^* for samples 1 and 3 in the vicinity of T_N. The average of the critical exponent is $\alpha = 0.103(3)$.

IV. DISCUSSION AND CONCLUSIONS

The AB_2O_6 family is a fascinating class of low-dimensional magnetic compounds. The two-sublattice antiferromagnetic structure exhibited by $CoSb_2O_6$, and some other AB_2O_6 compounds,[12] is particularly interesting, due to the 90° rotation of neighboring A-O-O-A chains along c. This unusual magnetic structure is partly responsible for the highly-anisotropic MCE.[12] Also responsible is the nature of the antiferromagnetism, as elucidated in the present work. Immediately above T_N, nearly 50% of the magnetic moments have lost their spin entropy, and are therefore in a state of partial order, where clusters of ordered 1D spins exist on the Co-O-O-Co chains.

The ordering at T_N must be such that the clusters align with regard to one another, combined with further ordering of the moments. This is similar to the picture put forth for $CuSb_2O_6$.[11] The feature in the heat capacity and thermal expansion coefficient, however, is a peak rather than the step-like feature exhibited in $CuSb_2O_6$.[11] This difference suggests a shorter correlation length associated with the magnetic order in $CoSb_2O_6$,[49] which leads to critical phenomena. The presented analysis is consistent with a continuous transition that is Ising-like. However, the transition's shape is easily affected by disorder, as revealed in Fig. 6, or the presence of magnetic field.[12] This supports the idea that the coupling between adjacent layers along c is weak and easily disrupted by perturbations or defects because of the 90° rotation of neighboring Co-O-O-Co chains along c.

Another important aspect is the presence of a very large linear term in C_P, which completely vanishes below T_N. This term must be associated with spin excitations in the paramagnetic state,[50,51] and it seems appropriate to attribute it to the local magnetic order that is present between T_N and 80 K. Unlike $CuSb_2O_6$, where a simple spin gap forms below T_N, the behavior of C_P for $CoSb_2O_6$ indicates the presence of antiferromagnetic magnons, with a gap. However, although the magnon term accounts for the majority of the δC_P curve below T_N, there is a minor residual portion that appears to be associated with unordered regions of the sample, which the analysis of ΔS_m reveals to be about 34% of the magnetic moments at the lowest measured temperature. The existence of significant magnetic disorder is revealing itself as a characteristic of the low-temperature magnetic ground state of these transition-metal-antimony oxides.[11,12]

The AFM phase transition in $CuSb_2O_6$ was interpreted as a spin-Peierls transition, with the addition that interchain coupling leads to 3D AFM order. We believe that the transition in $CoSb_2O_6$ has a similar origin, although here $S = 3/2$ on the transition-metal site. Theory has not yielded a strong conclusion regarding the existence of spin-Peierls transitions in $S = 3/2$ systems, but a qualitative argument has been advanced[52] and the possible existence of spin-dimers is suggested.[53] The spin gap observed in $CuSb_2O_6$ was $\Delta/k_B = 17.5$ K, which is about half of the Δ_2/k_B value reported here. However, the gapped region is more complex here, requiring two terms to obtain a reasonable fit. More work will be required to sort out the origin of these two gaps.

In conclusion, a broad range of temperature is observed where $CoSb_2O_6$ exhibits local antiferromagnetic order. This state is described simply as a collection of 1D ordered regions, but within 1D physics may be thought of more properly as a spin-liquid phase.[54] At $T_N = 13.45$ K, a transition to long-range antiferromagnetism occurs. This transition can be viewed as a 1D to 3D transition upon cooling through T_N, realized through alignment of the 1D regions, and further alignment of stray magnetic moments. Significant magnetic disorder remains to the lowest measurement temperatures. The transition at T_N appears to be continuous, and consistent with the 3D Ising universality class. The results provide an example of a crossover from 1D to 3D behavior resulting from 3D coupling among 1D magnetic chains of $S = 3/2$ magnetic moments that occurs below T_N.

Valuable discussions with Yi-Kuo Yu and Y. U. Idzerda are acknowledged. This material is based on the work supported by the National Science Foundation un-

der Contract No. DMR-0907036.

[1] S. Tomonaga, Prog. Theor. Phys. (Kyoto) **5**, 544 (1950).
[2] J. M. Luttinger, J. Math. Phys. **4**, 1154 (1963).
[3] T. Giamarchi, *Quantum Physics in One Dimension*, (Oxford: Clarendon Press, 2003).
[4] F. D. M. Haldane, J. Phys. C: Solid State Phys. **14**, 2585 (1981).
[5] D. Boies, C. Bourbonnais, and A.-M. S. Tremblay, Phys. Rev. Lett. **74**, 968, (1995).
[6] J. Kurmann, H. Thomas, and G. Müller, Physica **112**, 235 (1982).
[7] A. Nakua, H. Yun, J. N. Reimers, J. E. Greedan, and C. V. Stager, J. Solid State Chem. **91**, 105 (1991).
[8] M. Heinrich, H.-A. Krug von Nidda, A. Krimmel, A. Loidl, R. M. Eremina, A. D. Ineev, B. I. Kochelaev, A. V. Prokofiev, and W. Assmus, Phys. Rev. B **67**, 224418 (2003).
[9] S. M. Eicher, J. E. Greedan, and K. J. Lushington, J. Solid State Chem. **62**, 220 (1986).
[10] R. K. Kremer and J. E. Greedan, J. Solid State Chem. **73**, 579 (1988).
[11] A. Rebello, M. G. Smith, J. J. Neumeier, and B. D. White, Phys. Rev. B. **87**, 224427 (2013).
[12] A. B. Christian, S. H. Masunaga, A. T. Schye, A. Rebello, J. J. Neumeier, and Y.-K. Yu, Phys. Rev. B **90**, 224423 (2014).
[13] D. Kasinathan, K. Koepernik, and H. Rosner, Phys. Rev. Lett. **100**, 237202 (2008).
[14] J. M. Law, H.-J. Koo, M.-H. Whangbo, E. Brücher, V. Pomjakushin, and R. K. Kremer, Phys. Rev. B **89**, 014423 (2014)
[15] R. D. Johnson, K. Cao, L. C. Chapon, R. Fabrizi, N. Perks, P. Manuel, J. J. Jang, Y. S. Oh, S.-W. Cheong, and P. G. Radelli, Phys. Rev. Lett. **111**, 017202 (2013).
[16] M. Kato, K. Kajimoto, K. Yoshimura, K. Kosuge, M. Nishi, and K. Kakurai, J. Phys. Soc. Jpn. **71**, 187 (2002).
[17] A. M. Nakua and J. E. Greedan, J. Solid State Chem. **118**, 199 (1995).
[18] B. J. Gibson, R. K. Kremer, A. V. Prokofiev, W. Assmus, and B. Ouladdiaf, J. Magn. Magn. Mater. **272-276**, 927 (2004).
[19] E. M. da Silva Wheeler, Ph.D. thesis, Oxford University, 2007.
[20] M. Herak, D. Žilić, D. Matković-Čalogović, and H. Berger, cond-mat arXiv:1505.07405 (2015).
[21] H. Ehrenberg, G. Wltschek, J. Rodriguez-Carvajal, and T. Vogt, J. Magn. Magn. Mater. **184**, 111 (1998).
[22] J. N. Reimers, J. E. Greedan, C. V. Stager, and R. Kremer, J. Solid State Chem. **83**, 20 (1989).
[23] C. R. Michel, A. H. Martínez, and S. Jiménez, Sensors and Actuators B **132**, 45 (2008).
[24] A. V. Prokofiev, F. Ritter, W. Assmus, B. J. Gibson, and R. K. Kremer, J. Cryst. Growth **247**, 457 (2003).
[25] J. J. Neumeier, R. K. Bollinger, G. E. Timmins, C. R. Lane, R. D. Krogstad, and J. Macaluso, Rev. Sci. Instrum. **79**, 033903 (2008).
[26] A. Rebello, Z. C. M. Winter, S. Viall, and J. J. Neumeier, Phys. Rev. B **88**, 094420 (2013).
[27] K.-H. Hellwege and A. M. Hellwege, Landolt-Börnstein, New Series II/16 (Springer-Verlag, Heidelberg, 1986).
[28] M. Kato, A. Hatazaki, K. Yoshimura, and K. Kosuge, Physica B **281**&**282**,663 (2000).
[29] Stephen Blundell, *Magnetism in Condensed Matter* (Oxford University Press, Oxford, 2001).
[30] N. Ashcroft and N. Mermin, *Solid State Physics* (Holt, Rinehart and Winston, New York, 1976).
[31] I. B. Bersuker, *Electronic Structure and Properties of Transition Metal Compounds: Introduction to the Theory* (Wiley, New York, 2010).
[32] Y. Shirata, H. Tanaka, A. Matsuo, and K. Kindo, Phys. Rev. Lett. **108**, 057205 (2012).
[33] C. Kittel, *Introduction to Solid State Physics*, 7th ed. (Wiley, New York, 1996).
[34] J. C. Bonner and M. E. Fisher, Phys. Rev. **135**, A640 (1964).
[35] R. L. Carlin, *Magnetochemistry*, (Springer-Verlag, New York 1986), p. 106.
[36] The Hamiltonian used to obtain Equation 2 is given by $\mathbf{H} = -2J\mathbf{S}_{z1}\mathbf{S}_{z2} + g\mu_B H_z(\mathbf{S}_{z1} + \mathbf{S}_{z2})$, where boldfaced symbols are operators and z is the magnetic field direction, which is referred to as the $\|$ direction in the text.
[37] A. Tari, *The Specific Heat of Matter at Low Temperatures*, (Imperial College Press, London, 2003), p. 153.
[38] G. D. Barrera, J. A. O. Bruno, T. H. K. Barron, and N. L. Allan, J. Phys.: Condens. Matter **17**, R217 (2005).
[39] H. Winkelmann, E. Gamper, B. Buchner, M. Braden, A. Revcolevschi, and G. Dhalenne, Phys. Rev. B **51**, 12884 (1995).
[40] The poor thermal conductivity of fused quartz and sample-thermometer coupling provided only via helium gas can lead to features in μ if the warming rate is not constant.
[41] J. A. Souza, Y.-K. Yu, J. J. Neumeier, H. Terashita and R. F. Jardim, Phys. Rev. Lett. **94**, 207209 (2005).
[42] B. D. White, J. A. Souza, C. Chiorescu, J. J. Neumeier, and J. L. Cohn, Phys. Rev. B **79**, 104427 (2009).
[43] It is not uncommon for the regions of linearity to be limited to two decades in t for magnetic transitions, as is the case here. See: F. Grønvold, Pure & Appl. Chem. **47**, 251 (1976) and references therein.
[44] A. Pelissetto and E. Vicari, Phys. Rep. **368**, 549-727 (2002).
[45] L. P. Kadanoff, W. Götze, D. Hamblen, R. Hecht, E. A. S. Lewis, V. V. Palciauskas, M. Rayl, J. Swift, D. Aspnes, and J. Kane, Rev. Mod. Phys. **39**, 395 (1967).
[46] A. Kornblit and G. Ahlers, Phys. Rev. B **8**, 5163 (1973).
[47] P. F. Rebillot and D. T. Jacobs, J. of Chem Phys. **109**, 4009 (1998).
[48] A. J. Liu and M. E. Fisher, Physica A **156**, 35 (1989).
[49] V.L. Ginzburg, Fizika Tverdoga Tela **2**, 2031 (1960).
[50] Y.-K. Kuo, E. Figueroa, and J. W. Brill, Solid State Commun. **94**, 385 (1995).
[51] D. C. Johnston, R. K. Kremer, M. Troyer, X. Wang, A. Klümper, S. L. Bud'ko, A. F. Panchula, and P. C. Canfield, Phys. Rev. B **61**, 9558 (2000).
[52] D. Guo, T. Kennedy, and S. Mazumdar, Phys. Rev. B **41**, 9592 (1990).
[53] K. Gregor and O. I. Motrunich, Phys. Rev. B **76**, 174404

(2007).
[54] F. D. M. Haldane, Phys. Rev. B **25**, 4925 (1982).